Quantitative imaging of protein–protein interactions by multiphoton fluorescence lifetime imaging microscopy using a streak camera

R. V. Krishnan
A. Masuda
V. E. Centonze
B. Herman
University of Texas Health Science Center
Department of Cellular and Structural Biology
7703 Floyd Curl Drive
San Antonio, Texas 78229

Abstract. Fluorescence lifetime imaging microscopy (FLIM) using multiphoton excitation techniques is now finding an important place in quantitative imaging of protein–protein interactions and intracellular physiology. Recent developments in multiphoton FLIM methods are reviewed and a novel multiphoton FLIM system using a streak camera is described. An example of a typical application of the system is provided in which the fluorescence resonance energy transfer between a donor-acceptor pair of fluorescent proteins within a cellular specimen is measured. © *2003 Society of Photo-Optical Instrumentation Engineers.* [DOI: 10.1117/1.1577574]

1 Introduction

Detection of protein–protein interactions in living cells with high spatial and temporal resolution is a fundamental prerequisite for understanding cellular dynamics.[1] Visualization of specific probes by confocal and multiphoton imaging has improved spatial resolution in the context of cellular imaging in native, physiological conditions.[2,3] The implementation of fluorescence resonance energy transfer (FRET) detection in the optical microscope has extended the spatial detection limits of conventional fluorescence microscopy to a few nanometers—which is typically the magnitude of the distance between the interacting proteins. Measurement of FRET requires that there be a pair of fluorophores (donor and acceptor) between which there is nonradiative transfer of energy when they are in close proximity (~ 1 to 10 nm). The efficiency of energy transfer is determined by the distance separating the donor and acceptor molecules, the angular orientation of the fluorophores in space, overlap between the donor emission and acceptor excitation spectra, and the quantum yield of the donor in the absence of the acceptor.[4–6]

Many of the currently available FRET methods, such as sensitized emission, acceptor photobleaching, and concentration-dependent depolarization, utilize intensity-based measurements. These require the use of optical filters for spectral separation of donor-acceptor excitation and emission and can suffer from problems of spectral crosstalk. In addition, it is difficult to regulate the relative concentration of the donor and acceptor fluorophores, which in turn affects the efficiency of energy transfer, thus further complicating the measurement of cell component interactions using intensity-based FRET approaches. These methods also yield time-averaged information from an ensemble of interacting proteins (or other molecules) rather than the actual temporal kinetics of these interactions in real time. These constraints have led to the need to develop instrumentation that can measure FRET (protein–protein interactions) not only with high spatial resolution but also with a high degree of temporal resolution.

Fluorescence lifetime imaging microscopy (FLIM) allows dynamic information from cells to be obtained with high temporal resolution and provides an extra dimension of information (the fluorescent lifetime) in cellular imaging.[7–11] FLIM methods are insensitive to the concentration of the fluorophore, yet can still provide distinct lifetimes characteristic of the individual fluorophores attached to each protein (e.g., donor and acceptor). By measuring the changes in lifetime of the donor in the presence and in the absence of an acceptor molecule, it is possible to estimate the energy transfer efficiency, thereby allowing quantification of molecular interactions. By virtue of the fact that FLIM methods are devoid of aforementioned spectroscopic artifacts (as commonly encountered in intensity-based methods), the reliability in calculating quantitative FRET efficiencies is higher than in other methods. Besides FRET measurements, FLIM methods are also well suited for measuring intracellular physiology such as pH and ion concentration in real time.[12–16]

A variety of FLIM methods have been developed in the past decade for measuring various intracellular parameters by monitoring changes in the excited-state lifetime of fluorescence. These have been broadly classified into two major methods: time-domain and frequency-domain FLIM. In frequency-domain methods, the specimen is excited by a sinusoidally modulated wave of a certain frequency [$\sim$radio frequencies for nanosecond lifetimes; Fig. 1(a)]. The consequent fluorescence emission is also sinusoidally modulated, but with different phase and amplitude because of the time lag induced by "residence time" or the excited-state lifetime of the fluorophores. Generally a gain-modulated detector is used to determine the phase shift and amplitude demodulation from which the lifetimes of the fluorescent species are calculated.[17–19] Alternatively, in the case of time-domain methods, the specimen is illuminated with pulsed light and the
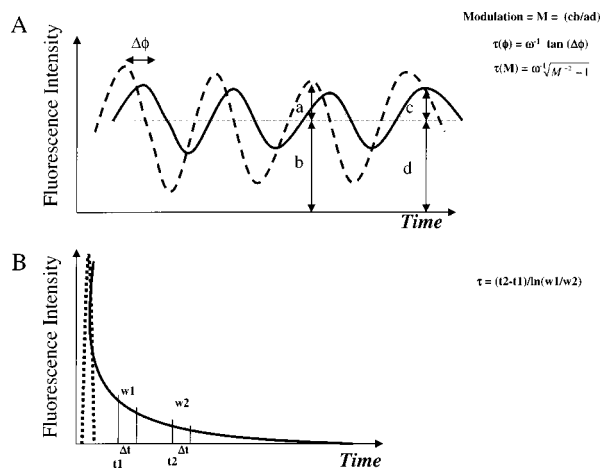
Fig. 1 (a) Schematic of the principle of frequency-domain lifetime imaging. ω is the modulation frequency. For single-component lifetimes of fluorescent species, the lifetimes $\tau(\phi)$ and $\tau(M)$ are the same, but differ if there is more than one lifetime component. (b) Schematic of the principle of time-domain lifetime imaging. Gated image intensifiers are set at different time windows ($w1, w2$) with a defined time interval (Δt), and the fluorescent lifetime is calculated according to the expression given above.

subsequent fluorescence emission decay is recorded by fast detectors [Fig. 1(b)]. By fitting the observed emission decay to an appropriate model, the lifetimes of the different fluorescent species within the specimen are extracted. Despite the availability of current FLIM methods for cell biological applications, a continual requirement that has pervaded this field is achieving high spatial and temporal resolution in live cell applications. Conventional time-domain FLIM methods such as multigate detection and single-photon counting can measure lifetimes as short as a few hundred picoseconds—a limitation imposed primarily by the detectors used in these systems. A recently developed imaging system determines the lifetime of fluorescence emission from multiphoton excitation imaging using a streak camera as the primary signal detector (streak-FLIM). Although streak cameras have been used in studies of semiconductor phenomena and picosecond spectroscopy, they have not yet been employed for FLIM in biomedical applications.[20–22] In this context, the present multiphoton-streak-FLIM system is unique and versatile, achieving excellent spatiotemporal resolution. To the best of our knowledge, it is the first of its kind developed for biomedical applications.

2 FLIM Methodology

The monoexponential decay scheme of a fluorescent molecule from its excited state can be represented by

$$I(t) = I_0 \exp(-t/\tau), \qquad (1)$$

where $I(t)$ is the measured intensity and I_0 is the intensity at time $t = 0$. The fluorescence lifetime, τ, is characteristic of the molecule and does not depend on its concentration within the specimen or on the excitation light characteristics (intensity, path length in the specimen, etc.). However, τ is sensitive to local environmental factors such as pH and ion concentration and is also sensitive to excited-state processes such as

quenching and energy transfer. As such, the measurement of changes in fluorescence lifetime under various experimental conditions functions as an indicator of alterations in intracellular physiology. For instance, FLIM offers a noninvasive way of measuring changes in H^+ or ion concentrations (e.g, Ca^{2+} oscillations) as well as being a reliable way of probing protein–protein interactions with high temporal resolution. In this article, we briefly review the different time-domain FLIM methods and describe in detail the development and biomedical application of the streak-FLIM system.

3 Time-Domain Detection Methods

3.1 Multigate Detection

In the simplest case of time-domain lifetime imaging, a gated microchannel plate image intensifier is used in conjunction with a CCD imaging camera.[23,24] By gating the image intensifier at different intervals (with a specified time window) along the exponential fluorescence decay profile, one can obtain a set of images of the actual decay of fluorescence during the excited-state lifetime [Fig. 1(b)]. It has been found that the photon utilization and time resolution of the multigate detection approach are still limited by the detector's performance. One also cannot avoid background noise arising from scattered fluorescence emission when an imaging (area) detector is used in multigate detection. Regardless of these limitations, the multigate detection FLIM methodology has been found to be very successful with single-photon excitation in recent years.[25,26] For multiphoton applications, it is imperative to use point-scanning detectors to eliminate background noise.

3.2 Single-Photon Counting

Photon-counting detectors are well suited for low-light level detection as well as for providing quantized pulses for every photon event.[27,28] This makes the measurement of lifetimes more accurate. However, these detectors suffer from poor dynamic range compared with their area detector counterparts. Regardless of this minor disadvantage, photon-counting devices have been found to be very reliable in terms of photon economy, rapid lifetime determination, and high temporal resolution. The limiting factor in achieving good temporal resolution is the transition-time spread (TTS) of the fast photomultiplier tubes (PMTs) used in these systems.

3.3 Streak-FLIM Imaging System

The essential feature of the streak camera is that it converts an optical 2-D image with spatial axes (x, y) into a streak image with temporal information and with the axes (x, t). A simplified picture of the streak imaging principle is demonstrated in (Fig. 2 and Fig. 3) and a brief description of the system is given in the following sections. For the complete technical details, see Ref. 30.

3.3.1 Light source

A mode-locked laser system (Coherent Inc. model Mira 900: titanium:sapphire gain medium pumped by a 10-W Verdi diode laser) was used in our experiments, providing ultrafast femtosecond pulses with a fundamental repetition rate of 76 MHz. To obtain the variable repetition rates for both intensity-based multiphoton imaging and for streak-FLIM detection, a
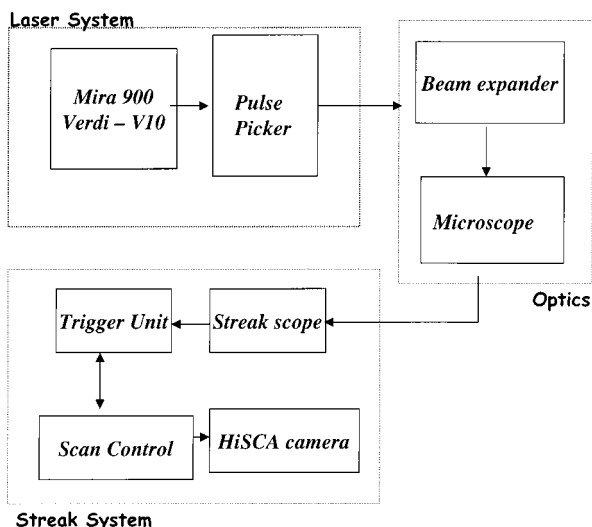
Laser System

Optics

Streak System

Fig. 2 The streak-FLIM imaging system is composed of the laser system (Coherent Mira 900 and Coherent Pulsepicker 9200), optics (Olympus IX-70 inverted microscope, FLIM optics), and the streak system (trigger unit, Streakscope, HiSCA Argus camera).

pulse picker, synchronized with the Mira excitation source, was employed. Precise optical alignment of the laser, the pulse picker, and the FLIM optics was essential to ensure negligible absorption and distortion of the excitation laser beam. The FLIM elements were optically aligned with respect to the optical axis of the microscope objective.

3.3.2 Microscope

The imaging system base is an Olympus IX70 inverted microscope. For intensity-based multiphoton images, the femtosecond-pulsed laser light was scanned into the left camera port via a modified FluoView X scan head. Nondescanned multiphoton emission was collected by a PMT in a custom-
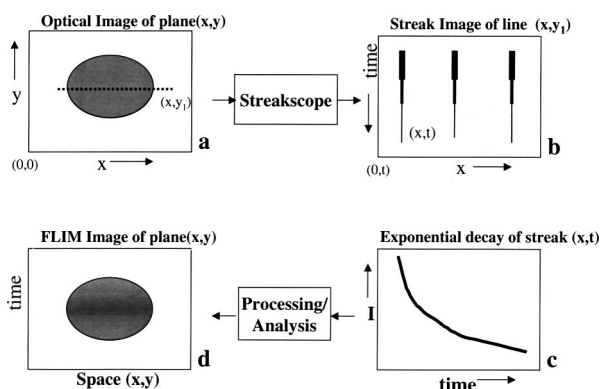

Fig. 3 A schematic of the principle of streak imaging. (a) A single line in the optical image with intensity information at every point is converted by the Streakscope into a streak image (b) with spatial information as the horizontal axis and time as the vertical axis. Every point (containing fluorescent molecules) along this line has an exponential decay profile as shown in (c). By scanning along the entire optical image (x, y plane), similar exponential decay profiles are produced that correspond to every point in the entire plane. These decay profiles are stored and then numerically processed to give a lifetime image as shown in (d). See text for more technical details.

designed housing mounted from the left side of the epifluorescence filter cassette. For streak-FLIM imaging, the femtosecond-pulsed laser light was scanned into the right camera port by the streak-FLIM unit. The fluorescence emission was directed back out through the same camera port and directed into the streak camera (C-4334, Hamamatsu Photonics K.K.). A specially designed $63\times$ (1.2 NA IR) water immersion objective was used for all the measurements reported in this paper. Experiments were done on either fixed cellular specimens mounted on standard microscope slides or on live cells grown on glass coverslips and maintained in appropriate media.

3.3.3 FLIM detection system

A microchannel plate (MCP) was used in the streak-FLIM detection path. The Streakscope (Hamamatsu, C4334) has a temporal resolution of $\sim$50 ps and a very small photocathode dark current. This facilitates a high signal-to-noise ratio (SNR) for measuring even weak fluorescence signals. The electrical output of the MCP is converted to an optical output (streak image) on a phosphor screen. This image is then output to a fast CCD camera (Hamamatsu, Argus/HiSCA) that is fiber optically coupled to the Streakscope. An important feature of the HiSCA camera is that it employs a CCD chip that offers exceptionally high-speed and high-sensitivity detection ($\sim$2% quantum efficiency). The 12-bit image depth enables even minute changes in fluorescence intensity to be detected. A variable sampling rate (1 to 24 frames/s) and spatial resolution allow the flexibility to detect fast photon events and low light signals. A maximum sampling rate of $\sim$500 frames/s can be achieved with the HiSCA camera for single-wavelength fluorescence measurements, which is more than ten times higher than the normal video rate. Faster frame acquisition can be achieved by binning the pixels. Binning in the x-axis decreases spatial resolution while binning in the t (time) axis decreases the temporal resolution [Fig. 3]. Thus a compromise between the speed of the data acquisition and the required resolution must be made for each measurement. Unbinned, the maximum number of pixels of the CCD camera is 658×494; a maximum binning of 32×32 can be achieved. The FLIM data acquisition is governed by AquaCosmos software (Hamamatsu) and the streakscope output signal is processed by AquaCosmos software to convert the exponential decay into a mean lifetime value on a per pixel basis, thus creating an FLIM image display.

3.4 System Calibration

Standard solutions of various fluorescent dyes were used for calibration of the system and for optimizing the relevant parameters for a typical measurement. Rhodamine 6G and rose bengal solutions were prepared in different solvents as detailed in Table 1. These dyes are reported to have monoexponential fluorescent decays and therefore display a single lifetime.[29] The choice of standard dyes also allowed calibration of the system for measurement of lifetime values ranging from a few hundred picoseconds to a few nanoseconds. Table 1 gives the calculated lifetime values for these solutions obtained with the FLIM streakscope system and compares these values with values reported in the literature for the same fluorophore solutions. There is a very good agreement between

Table 1 Measured lifetimes in the streak-FLIM system.

Samples		Measured Lifetimes		Literature	
		τ (ns)	Standard Deviation (ns)	τ (ns)	Reference
Calibration probes	Rhodamine 6G/ethanol	2.97	0.14	3.0	29
	Rose bengal/acetone	2.22	0.13	2.4	29
	Rose bengal/ethanol	0.74	0.04	0.8	29

Note: The standard solutions were prepared by dissolving the dye powders in different solvents and diluted stocks were prepared for calibration. Calculated lifetime values did not change with the concentration of the dye in the nominal range of a few hundred nanomoles to a few hundred micromoles. All the measurements were carried out at around 200 μM concentration for system calibration. Raw streak images were obtained and the mean lifetimes were calculated by the methods described in the text. Monoexponential decays were assumed for all the calibration samples as reported in literature, and the values reported here are all mean lifetime values. Standard deviations were obtained by fitting the lifetime histograms to normal distribution.

the calculated lifetimes and those in the literature, demonstrating the accuracy of lifetime determination of the streak-FLIM system. Accuracy of the lifetime measurements is largely governed by the uniformity of the FLIM images. Lifetime images of the standard solutions that we employed exhibited a high degree of uniformity and thus provided high accuracy in the calculations of lifetime. Reproducibility between two measurements in the same specimen was found to be >99% in standard solutions. However, for cellular specimens, the variability in cellular expressions as well as the inevitable photobleaching artifacts can restrict the reproducibility. A more detailed description of the instrument's performance and signal and noise issues can be found in Ref. 30.

3.5 Biological Applications

Cyan and yellow fluorescent proteins (CFP/YFP) are mutated forms of the wild-type green fluorescent protein and are employed as a donor-acceptor pair in many FRET experiments.[31,32] Energy transfer can be manifested in many ways, such as a reduction in donor emission fluorescence, sensitized fluorescence emission of the acceptor, or a reduction in donor lifetime. Of all the different FRET methods, measuring FRET by measuring the changes in donor lifetime has been reported to be more reliable owing to its relative insensitivity to the spectroscopic artifacts commonly encountered in intensity-based measurements. In this section we give a typical cellular application of the streak-FLIM system in studying caspase activity in single cells. Baby hamster kidney (BHK) cells were transiently transfected with a mitochondrially targeted DNA construct (mC2Y) that links CFP and YFP by an amino acid encoding a caspase-2 (VDVAD) recognition sequence.[33] Under identical conditions of growth and transfection, a batch of cells was exposed to the broad-range caspase activator *tert*-butyl hydrogen peroxide (*t*BOOH: 50 μM) for 4 h at 37 °C in order to induce oxidative stress in mitochondria. Experiments were carried out under identical imaging conditions for all of the specimens. It is expected that the close proximity of CFP and YFP molecules in the intact caspase-2 substrate would lead to significant energy transfer in the mC2Y specimens. However, induction of

caspase-2 activity in *t*BOOH-treated mC2Y specimens should lead to cleavage of the substrate, thereby altering the spatial relationship between the CFP and YFP molecules and decreasing the extent of energy transfer in these specimens. We measured lifetimes of the CFP in both the *t*BOOH-treated and untreated cells and calculated the change in energy transfer efficiency in these two situations.

For measurements of CFP fluorescence lifetime, the femtosecond-pulsed laser was tuned to 840 nm. To select for emission from CFP only, the fluorescent signal passed through a 480/30 emission filter (Chroma Inc.) placed before the Streakscope. Donor lifetime images were calculated using AquaCosmos software. Figure 4 shows the (CFP) lifetime images of the mC2Y and mC2Y+*t*BOOH specimens. The mC2Y specimen shows punctate mitochondrial expression of CFP, whereas there is an observable morphological change in the *t*BOOH-treated specimen. This morphological change (the cell becomes more rounded), together with the diffuse fluorescence in Fig. 4(b), can be attributed to oxidative stress induced by *t*BOOH and the consequent induction of apoptosis in the cell. As can be seen from the lifetime histogram, the mean lifetime of the mC2Y specimen is about 2 ns, whereas that of the *t*BOOH-treated mC2Y specimen is about 2.28 ns. This increase in lifetime is a clear manifestation of loss of energy transfer between CFP and YFP molecules in the *t*BOOH-treated mC2Y specimen compared with the untreated mC2Y specimen, where the molecules are held intact by the intervening caspase-2 peptide sequence. This indicates that a significant mitochondrial caspase activity is induced by oxidative stress. As a positive control for FRET measurements, we used DNA constructs encoding mitochondrially targeted CFP-polyglycine-YFP (mCGY) in BHK fibroblast cells and imaged under conditions identical to those for our experimental studies (mC2Y). Both these specimens exhibited average lifetimes of ~2.0 ns. Upon treatment with caspase activator, *t*BOOH, only the mC2Y specimen showed a 15% increase in average lifetime, whereas the mCGY specimen showed less than a 5% change in lifetime. This proved that what we see as a change in lifetime in the mC2Y specimen upon *t*BOOH treatment is essentially due to caspase activity. It is also in-
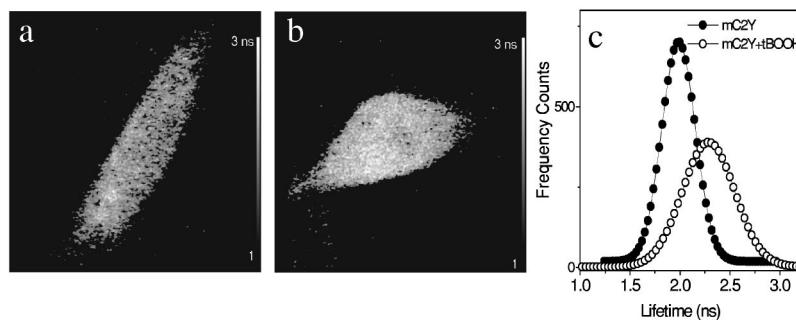
Fig. 4 Fluorescence lifetime images of baby hamster kidney cells transfected with a mitochondrially targeted DNA construct (mC2Y) that links CFP and YFP via an amino acid sequence encoding a caspase-2 recognition site. (a) untreated mC2Y; (b) mC2Y treated with 50 M tBOOH for 4 h; (c) lifetime histogram for both specimens. The laser output from Mira 900 (76-MHz repetition rate; 840-nm wavelength; ∼200-fs pulse width) is rendered to the pulse picker, which steps down the repetition rate to 500 kHz optimized for triggering the Streakscope. The average power at the entrance of the FLIM optics is 8 mW. The 12-bit streak images were obtained in the 1×32 binning condition. Exposure times for imaging (∼195 ms per single line) were optimized to minimize photobleaching during data acquisition. The lifetime images were calculated from the raw streak images by AquaCosmos software (Hamamatsu). An intensity threshold criterion of about 10% of the maximum dynamic range was used in calculation of lifetime images, and the final images were median filtered. The lifetime histograms shown were plotted for the entire cells. The mean lifetime of the mC2Y specimen was 1.98 ns, whereas that of tBOOH-treated mC2Y specimen was 2.28 ns.

triguing to note that the lifetime distribution in the tBOOH-treated specimen is much broader than that of the untreated mC2Y specimen. This can be interpreted as representing nonuniform caspase cleavage activity within the cell.

Some of the caspase-2 substrates were cleaved when the lifetime measurement was made, while other substrates remained intact. This would cause a wide distribution in the extent of energy transfer spatially within the cell and manifest itself as a wider distribution in the measured lifetime in the tBOOH-treated specimen. Although it would be interesting to analyze these histograms by multicomponent lifetime models, only a single-component Gaussian model was adopted in the present analysis. Furthermore, at 4 h post-tBOOH treatment, only about 50% of the cells showed changes in lifetime upon tBOOH treatment. Different cells in an ensemble would be at different stages of apoptosis at any one time. Since the fixation of the cells was done at a single time point after the tBOOH treatment, it is expected that not all the cells would exhibit apoptotic changes in lifetime measurement. It is also possible that there exists a substantial population of uncleaved caspase-2 substrate, even in the tBOOH-treated specimen because this substrate is being constitutively expressed.

The energy transfer efficiency can be calculated from the expression $E = 1 - (\tau_{DA}/\tau_D)$, where τ_{DA} and τ_D are the lifetimes of the donor in the presence and in the absence of acceptor, respectively. In the present case, τ_{DA} and τ_D represent the mean lifetimes of CFP in the untreated and tBOOH-treated specimens, respectively. From the fitting of mean lifetime histograms in both the specimens, the change in energy transfer efficiency in the above example was calculated to be ∼15%.

We have taken care to ensure that the calculated lifetime values are not affected by photobleaching artifacts or autofluorescence contributions. Imaging conditions were optimized for minimal photobleaching so as to get reproducible lifetime values from the same region of the cell in consecutive scans. It was observed earlier that autofluorescence from fibroblast cells has typical lifetime values of about 2.2 ns.[15] We measured the streak images of nontransfected cells and found that

the maximum contribution to fluorescence intensity from autofluorescence is less than 5% of that observed in transfected cells. We have thresholded the streak-FLIM image intensity values above this value in our lifetime calculations in order to remove the ambiguity of a possible contribution of autofluorescence to the observed lifetime. It is also worth mentioning that autofluorescence contributions have been found to be less using multiphoton excitation.[34]

The demonstration of reliable FRET measurement using multiphoton lifetime imaging combined with a streak camera opens up new possibilities for quantitative imaging of protein–protein interactions in living cellular systems. Since the requirement is to measure only donor lifetime in all the specimens, the problem of spectral crosstalk is overcome. However, it is advisable to measure the lifetime of a donor in the absence of an acceptor under identical imaging conditions that can then serve as a control for non-FRET conditions.

In recent years there has been an upsurge in the quantitative imaging of molecular interactions in addition to the intensity-dependent visualization of intracellular probes. Improvements in fluorescence techniques such as confocal, multiphoton microscopy and other energy transfer methods have yielded valuable spatial and spectral information pertinent to submicron molecular interactions. Lifetime imaging methods offer improved temporal resolution in fluorescence imaging, thereby incorporating an additional experimental parameter. Although single-photon FLIM techniques have been in use for many years, it is expected that the combination of multiphoton excitation and FLIM methods will yield an enhancement in spatiotemporal resolution and reduce overall phototoxicity and thereby improve our understanding of molecular interactions.

References

1. *Methods in Cellular Imaging*, A. Periasamy, Ed., Oxford University Press, New York (2001).
2. J. B. Pawley, *Handbook of Biological Confocal Microscopy*, Plenum, New York (1995).

3. K. Konig, ''Multiphoton microscopy in life sciences,'' *J. Microsc.* **200**, 83–104 (2000).

4. R. M. Clegg, ''Fluorescence resonance energy transfer,'' *Curr. Opin. Biotechnol.* **6**, 103–110 (1995).

5. P. R. Selvin, ''The renaissance of fluorescence resonance energy transfer,'' *Nat. Struct. Biol.* **7**, 730–734 (2000).

6. R. V. Krishnan, R. Varma, and S. Mayor, ''Fluorescence methods to probe nanometer scale organization of molecules in living cell membrane,'' *J. Fluorescence* **11**, 211–226 (2001).

7. J. R. Lakowicz, ''Emerging applications of fluorescence spectroscopy to cellular imaging: lifetime imaging, metal-ligand probes, multiphoton excitation and light quenching,'' *Scanning Microsc. Suppl.* **10**, 213–224 (1996).

8. T. Oida, Y. Sako et al., ''Fluorescence lifetime imaging microscopy (flimscopy). Methodology development and application to studies of endosome fusion in single cells,'' *Biophys. J.* **64**(3), 676–685 (1993).

9. A. Squire and P. I. Bastiaens, ''Three-dimensional image restoration in fluorescence lifetime imaging microscopy,'' *J. Microsc.* **193**(Pt. 1), 36–349 (1999).

10. A. Squire, P. J. Verveer et al., ''Multiple frequency fluorescence lifetime imaging microscopy,'' *J. Microsc.* **197**(Pt. 2), 136–149 (2000).

11. A. H. Clayton, Q. S. Hanley et al., ''Dynamic fluorescence anisotropy imaging microscopy in the frequency domain (rFLIM),'' *Biophys. J.* **83**(3), 1631–49 (2002).

12. H. Szmacinski and J. R. Lakowicz, ''Possibility of simultaneously measuring low and high calcium concentrations using Fura-2 and lifetime-based sensing,'' *Cell Calcium* **18**(1), 64–75 (1995).

13. T. W. Gadella Jr. and T. M. Jovin, ''Oligomerization of epidermal growth factor receptors on A431 cells studied by time-resolved fluorescence imaging microscopy. A stereochemical model for tyrosine kinase receptor activation,'' *J. Cell Biol.* **129**(6), 1543–1558 (1995).

14. P. J. Verveer, F. S. Wouters et al., ''Quantitative imaging of lateral ErbB1 receptor signal propagation in the plasma membrane,'' *Science (Washington, DC, U.S.)* **290**(5496), 1567–1570 (2000).

15. M. A. van Zandvoort, C. J. de Grauw et al., ''Discrimination of DNA and RNA in cells by a vital fluorescent probe: lifetime imaging of SYTO13 in healthy and apoptotic cells,'' *Cytometry* **47**(4), 226–235 (2002).

16. M. Elangovan, R. N. Day et al., ''Nanosecond fluorescence resonance energy transfer-fluorescence lifetime imaging microscopy to localize the protein interactions in a single living cell,'' *J. Microsc.* **205**(Pt. 1), 3–14 (2002).

17. T. French, P. T. So et al., ''Two-photon fluorescence lifetime imaging microscopy of macrophage-mediated antigen processing,'' *J. Microsc.* **185**(Pt. 3), 339–353 (1997).

18. P. J. Verveer, A. Squire et al., ''Improved spatial discrimination of protein reaction states in cells by global analysis and deconvolution of fluorescence lifetime imaging microscopy data,'' *J. Microsc.* **202**(Pt. 3), 451–456 (2001).

19. P. J. Verveer, A. Squire et al., ''Global analysis of fluorescence lifetime imaging microscopy data,'' *Biophys. J.* **78**(4), 2127–2137 (2000).

20. T. Tahara and H. O. Hamaguchi, *Appl. Spectrosc.* **47**, 391 (1993).

21. M. Heya, S. Fujioka, H. Shiraga, N. Miyanaga, and T. Yamanaka, *Rev. Sci. Instrum.* **72**, 755 (2001).

22. U. Neuberth, L. Walter, G. von Freymann, B. Dal Don, H. Kalt, M. Wegener, G. Khitrova, and H. M. Gibbs, *Appl. Phys. Lett.* **80**, 3340 (2002).

23. M. Straub and S. W. Hell, *Appl. Phys. Lett.* **73**, 1769 (1998).

24. H. C. Gerritsen, M. A. H. Asselbergs, A. V. Agronskaia, and W. G. J. A. H. M. Van Sark, ''Fluorescence lifetime imaging in scanning microscopes: acquisition speed, photon economy and lifetime resolution,'' *J. Microsc.* **206**, 218–224 (2002).

25. M. J. Cole, J. Siegel et al., ''Time-domain whole-field fluorescence lifetime imaging with optical sectioning,'' *J. Microsc.* **203**(Pt. 3), 246–257 (2001).

26. J. Sytsma, J. M. Vroom, C. J. de Grauw, and H. C. Gerritsen, ''Time-gated lifetime imaging and micro-volume spectroscopy using two-photon excitation,'' *J. Microsc.* **191**, 39–51 (1998).

27. A. Schonle, M. Glatz, and S. W. Hell, ''Four-dimensional multiphoton microscopy with time-correlated single-photon counting,'' *Appl. Opt.* **39**, 6306–6311 (2000).

28. W. Becker, A. Bergmann, and G. Weiss, ''Lifetime imaging with the Zeiss LSM-510,'' *Proc. SPIE* **4620**, 30–35 (2002).

29. A. Periasamy, P. Wodnicki, X. F. Wang, S. Kwon, G. W. Gordon, and B. Herman, ''Time-resolved fluorescence lifetime imaging microscopy using a picosecond-pulsed tunable dye laser system,'' *Rev. Sci. Instrum.* **67**, 3722 (1996).

30. R. V. Krishnan, H. Saitoh, H. Terada, V. E. Centonze, and B. Herman, ''Development of a multiphoton fluorescence lifetime imaging microscopy (FLIM) system using a streak camera,'' *Rev. Sci. Instrum.* **74**, 2714–2721 (2003).

31. J. M. Tavare, L. M. Fletcher, and G. I. Welsh, ''Using green fluorescent protein to study intracellular signaling,'' *J. Endocrinol.* **170**, 297–306 (2001), and references therein.

32. A. G. Harpur, F. S. Wouters et al., ''Imaging FRET between spectrally similar GFP molecules in single cells,'' *Nat. Biotechnol.* **19**(2), 167–169 (2001).

33. N. P. Mahajan, D. C. Harrison-Shostak, J. Michaux, and B. Herman, ''Novel mutant green fluorescent protein protease substrates reveal the activation of specific caspases during apoptosis,'' *Chem. Biol.* **6**, 401–409 (1999).

34. K. Konig, P. T. So et al., ''Two-photon excited lifetime imaging of autofluorescence in cells during UVA and NIR photostress,'' *J. Microsc.* **183**(Pt. 3), 197–204 (1996).